Enhanced CO_2 Sensing by Oxygen Plasma Treated Perovskite-Graphene Nanocomposites

Juan Casanova-Chafer[1,2], Rocio Garcia-Aboal[3], Eduard Llobet[2,3], Pedro Atienzar[4]

[1] Chimie des Interactions Plasma Surface, CIRMAP, Université de Mons, 7000 Mons, Belgium

[2] Universitat Rovira i Virgili, 43007 Tarragona, Spain

[3] Research Institute in Sustainability, Climate Change and Energy Transition (IU-RESCAT), 43480 Vila-seca, Spain

[4] Instituto de Tecnología Química, CSIC-UPV, Universitat Politècnica de València, 46022 Valencia, Spain

Keywords: perovskite, graphene, oxygen plasma, CO_2, gas sensor

Abstract

Carbon dioxide (CO_2) is a major greenhouse gas responsible for global warming and climate change. The development of sensitive and selective CO_2 sensors is crucial for environmental and industrial applications. This paper presents a novel CO_2 sensor based on perovskite nanocrystals immobilized on graphene and functionalized with oxygen plasma treatment. The impact of this post-treatment method was thoroughly investigated using various characterization techniques, including Raman spectroscopy, XRD, and XPS. The detection of CO_2 at parts per million (ppm) levels demonstrated that the hybrids subjected to 5 minutes of oxygen plasma treatment exhibited a three-fold improvement in sensing performance compared to untreated layers. Consequently, the CO_2 sensing capability of the oxygen-treated samples showed a limit of detection (LOD) and limit of quantification (LOQ) of 6.9 ppm and 22.9 ppm, respectively. These levels meet the requirements for many real-world applications, underscoring the high potential of the developed sensor layers. Furthermore, the influence of ambient moisture on CO_2 sensing performance was also evaluated, revealing a significant effect of oxygen plasma treatment.

1. Introduction

Carbon dioxide (CO_2), a major greenhouse gas is responsible for global warming and climate change. The CO_2 concentration in the atmosphere has risen from approximately 280 ppm during pre-industrial times to about 410 ppm in 2019,[1] primarily due to human activities such as fossil fuel combustion, deforestation, and land use changes.[2] Despite its negative impact on the environment, CO_2 finds applications in various fields including fire suppression,[3] medical settings like anesthesia or computed tomography,[4] carbonation of beverages,[5] and agriculture for enhancing plant growth.[6] However, exposure to high levels of CO_2 can have adverse effects on humans, including dizziness, respiratory issues, and circulatory disorders.[7] More recently, CO_2 gas sensors have been extensively used in indoor environments such as schools and offices due to the COVID-19 pandemic.[8] This is because elevated CO_2 levels in enclosed spaces indicate poor ventilation, increasing the risk of respiratory infections like COVID-19 and influenza.[9] In this context, the CO_2 sensors have emerged as powerful tools for detecting when indoor environments require adequate ventilation.[10] Therefore, monitoring and controlling the emission and accumulation of CO_2 are crucial in mitigating its adverse effects on both the environment and human health across various situations.

Researchers have reported various types of CO_2 gas sensors, including optical sensors,[11] surface acoustic wave sensors,[12] and quartz crystal microbalance sensors.[13] However, chemical resistive

(chemiresistive) sensors have gained significant research interest due to their user-friendliness, simple readouts, and cost-effectiveness.[14] Most chemiresistive sensors have focused on metal oxides (MOx) such as ZnO, SnO, or WO_3, but achieving optimal CO_2 sensing requires operating temperatures in the range of several hundred degrees Celsius.[15–17] These high operating temperatures pose challenges in terms of power consumption, cost as they require heating elements and more complex circuitry, and long-term stability, as the materials may undergo phase changes or agglomeration into larger entities through coalescence effects.[18]

Alternatively, integrating carbon-based nanomaterials into chemiresistive sensors has been proven as a viable option for detecting gaseous analytes at room temperature.[19] This approach offers advantages such as reduced power consumption, lower device cost, and improved long-term stability of the sensitive film.[20] However, pristine carbon nanomaterials like graphene or carbon nanotubes face challenges of sensitivity and selectivity due to their inert surfaces.[21] These challenges are particularly amplified when detecting a relatively inert and linear gas such as CO_2.[22] It is worth noting that there have been few studies focused on detecting CO_2 compared to other compounds like NO_2. This is because CO_2, due to its inert properties, exhibits limited adsorption and diffusion rates on sensor surfaces. Additionally, the charge transfer and adsorption energies associated with CO_2 are significantly lower compared to gases like SO_2 or CO.[23] Moreover, as mentioned earlier, the sensitization of metal oxides to CO_2 is highly dependent on elevated operating temperatures.[24] Hence, the detection of CO_2 at ambient temperature to achieve durable, inexpensive, and low-powered devices poses a major challenge.

To address these challenges, this paper presents a novel approach utilizing oxygen-plasma treated graphene-perovskite composites to achieve unprecedented sensing performance at room temperature. Graphene, a two-dimensional nanomaterial with a large surface area, high conductivity, and excellent mechanical properties,[25] is used as a support for halide perovskite nanocrystals (NCs) to enhance sensitivity.[26] While perovskite NCs decorating graphene sheets have been previously proposed for detecting reactive gases such as NO_2 or NH_3,[27] detecting CO_2 presents a greater challenge. To overcome this, an oxygen plasma pre-treatment is employed to create defects and introduce oxygen-containing functional groups (such as hydroxyls, carbonyls, carboxyl, and epoxy groups) on the graphene surface, enabling stronger interactions with analytes such as CO_2 molecules.[28] These modifications are expected to enhance the affinity of the interactions with perovskite nanocrystals. Previous studies have shown that oxygen plasma treatment improves the sensing performance of graphene by inducing defect engineering and grafting oxygen functional groups onto the surface.[29,30]

In terms of lead halide perovskite NCs, oxygen plasma treatment has been demonstrated to improve properties such as absorbance, photoluminescence (PL) intensity, carrier concentration and mobility.[31] These parameters have the potential to impact the sensing performance. Specifically, this study focuses on an inorganic perovskite ($CsPbBr_3$), which has been shown to be more resistant to oxygen plasma compared to organic counterparts.[32] However, here we explore, for the first time, the use of an oxygen-plasma treated perovskite-graphene nanocomposite for gas sensing applications.

2. Experimental Methods

2.1. NCs Synthesis

The $CsPbBr_3$ nanocrystals were synthesized adapting the protocol proposed by L. Protesescu *et al.*[33] Cs_2CO_3 (814 mg), octadecene (40 mL), and oleic acid (2.5 mL) were mixed in a 3-neck flask.

The solution was heated to 120ºC for 1 hour and then further heated to 150ºC under a nitrogen atmosphere to complete the reaction between Cs_2CO_3 and oleic acid.

In parallel, another solution was prepared by mixing $PbBr_2$ (69 mg) and ODE (5 mL). The solution was dried under vacuum at 120ºC for 1 hour. Then, dried oleylamine (500 µL) and OA (500 µL) were injected. Once solubilization was complete, the temperature was increased to 140ºC, and a solution of Cs-oleate (0.4 mL) was quickly injected. After 5 seconds, the final solution was cooled in an ice bath, and 5 mL of Tert-butyl alcohol (tBuOH) was added to aid in the crystallization of the NCs. The nanocrystals were isolated by centrifugation (6000 rpm, 5 min) and redispersed in hexane.

2.2. Sensor preparation

A graphene solution in hexane (0.5 mg/mL) was prepared using graphene nanoflakes from Strem Chemicals, Inc. (US). The solution was subjected to pulsed sonication (1s on/2s off) at 280 W for 90 minutes to achieve proper exfoliation of the graphene. Subsequently, perovskite NCs (5% wt.) were added to the solution, and the nanomaterials were mixed in an ultrasonic bath for 1 hour. Finally, the resulting graphene flakes decorated with perovskite NCs were deposited onto alumina substrates containing screen-printed platinum interdigitated electrodes using a spray pyrolysis technique.

2.3. Plasma treatment

The oxygen plasma treatment was performed using a low-pressure plasma instrument called FEMTO (Diener). The perovskite@graphene sensor was placed in the plasma chamber, which was initially degassed under vacuum for 30 minutes. Then, an O_2 flow was introduced to achieve a stable pressure of 4 mbar. An optimized potential of 50 W and short treatment times of 5 and 15 minutes were found to be appropriate for generating perovskite defects. Finally, the plasma chamber was subjected to vacuum for 5 minutes and then refilled with Ar until atmospheric pressure was reached.

2.4. Gas sensing measurements

The gas sensors were placed inside a sealed Teflon chamber with a volume of 35 cm^3. This chamber was connected to a gas mixing and delivery system that utilized calibrated gas cylinders and pure dry air (Air Premier purity: 99.999%) as the carrier gas. The resistance of the sensors was monitored using a multimeter (HP 34972A, Agilent), and changes in resistance were recorded as different concentrations of gases were applied.

To ensure realistic experimental conditions and minimize power consumption, the total flow rate was adjusted to a low value of 100 mL/min using a combination of mass-flow controllers (Bronkhorst High-Tech B.V.) and electrovalves. Prior to exposure to a specific concentration of a gaseous species, the sensors were allowed to stabilize under dry air for 15 minutes. The sensor responses to different concentrations were recorded by gradually diluting the gases, and the sensor response was expressed as a percentage change in resistance ($\Delta R/R_0$), where ΔR represents the resistance changes observed over a 5-minute period of gas exposure, and R_0 is the baseline resistance of the sensor in air.

To investigate the gas-sensing performance in the presence of humidity, it was employed a controller evaporator mixer from Bronkhorst High-Tech B.V. This device enabled the controlled introduction of humidity into the testing environment during specific measurements. By

incorporating ambient moisture, it is possible to assess the impact of humidity on the sensor response and evaluate its influence on the sensing performance.

2.5. Material Characterization

The morphology of the perovskite NCs was studied using a *JEOL JEM 2100F* High-Resolution Transmission Electron Microscope (HRTEM). The X-Ray Diffraction (XRD) patterns were recorded on a Philips X'PERT diffractometer equipped with a proportional detector and a secondary graphite monochromator. The data was collected stepwise over the range 2θ = 2–20°, with steps of 0.02° and an accumulation time of 20 s/step. Cu Kα radiation (λ = 1.54178 Å) was used as the X-ray source. Raman spectrometry was performed using an instrument from Renishaw, Inc., coupled to a confocal Leica DM2500 microscope. The laser used had a wavelength of 514 nm. The perovskite-graphene nanocomposite was analyzed using a *Zeiss Gemini SEM 500* High-Resolution Field Emission Scanning Electron Microscope (HRFESEM). The chemical surface was studied using X-ray photoelectron spectroscopy (XPS) with a VERSAPROBE PHI 5000 instrument equipped with a Monochromatic Al Kα X-ray source from Physical Electronics Inc. The energy resolution was 0.6 eV, and a dual beam charge neutralization system consisting of an electron gun (~1 eV) and an Argon ion gun (<10 eV) was used to compensate for built-up charge during the measurements. All XPS binding energies were calibrated to the Au 4f7/2 peak at 84.0 eV.

3. Results and discussion

3.1. Characterization of perovskite-graphene nanocomposites

The morphology and size of the $CsPbBr_3$ nanocrystals were studied using HRTEM. The nanomaterial was dispersed in hexane through ultrasonication, and a drop of the dispersion was deposited onto a carbon-coated copper grid and dried at room temperature. Figure 1a shows that the perovskites exhibit a square shape with homogeneous size. To obtain the size distribution, more than 100 perovskite nanocrystals were analyzed, as shown in Figure S1. The majority of the NCs are between 8 and 13 nanometers in lateral dimensions, resulting in an overall average size of 10.9 ± 1.7 nm. Figure 1b reveals the high crystallinity of the synthesized $CsPbBr_3$ NCs, displaying an interplanar distance of about 2.9 Angstrom.

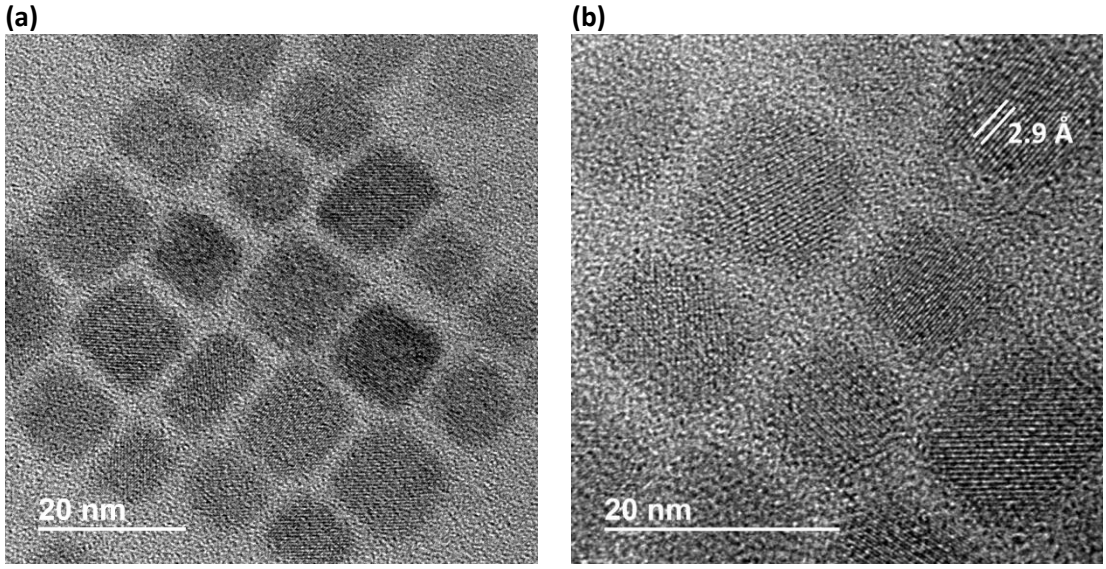

Figure 1. HRTEM images showing an example of $CsPbBr_3$ nanocrystals (a) and their high crystallinity and interplanar distance (b).

The HRFESEM images of the perovskite-graphene nanocomposite results can be observed in Figure S2. Figure S2a shows a highly porous graphene surface. Previous studies[34] have reported that bare graphene has a BET area of 730 m^2/g. To observe the perovskite nanocrystals, a Back-Scattered Electron (BSE) detector was used, as shown in Figure S2b, revealing a suitable distribution of nanocrystals along the graphene surface.

To confirm that the oxygen plasma treatment does not destroy the perovskite NCs, an analysis was performed by exposing isolated $CsPbBr_3$ to the same plasma experimental process and analyzing it by XRD. Figure 2a demonstrates the absence of significant changes in the peaks, even after 15 minutes of oxygen plasma treatment, indicating that the orthorhombic structure of $CsPbBr_3$ is retained. This confirms that under the applied experimental conditions, the oxygen plasma is almost harmless to the perovskites, consistent with similar works.[32]

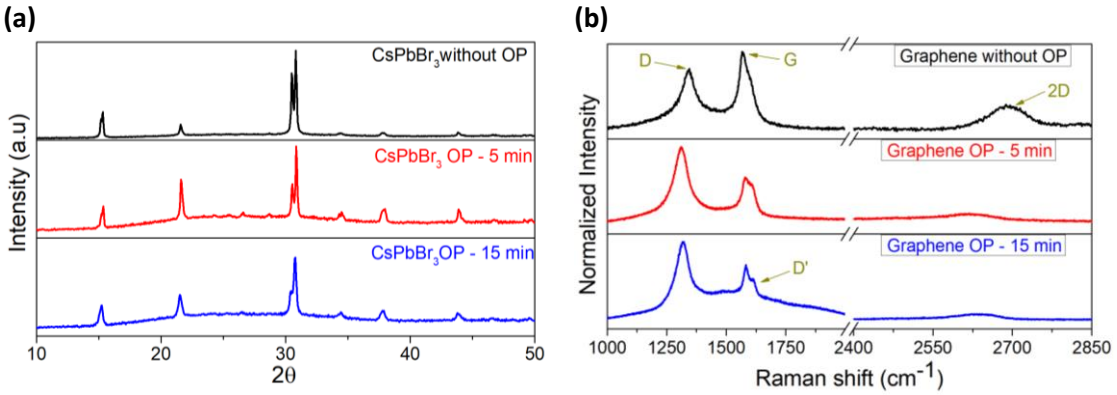

Figure 2. (a) Comparison of the XRD patterns of $CsPbBr_3$ NCs without exposure to oxygen plasma (black line), irradiated for 5 minutes (red line), and irradiated for 15 minutes (blue line). (b) Comparison of Raman spectroscopy for bare graphene without exposure to oxygen plasma (black line), and irradiated for 5 and 15 minutes (red and blue lines, respectively).

The crystallinity and defects of graphene before and after the plasma treatment were evaluated using Raman spectroscopy, as shown in Figure 2b. Pristine graphene exhibits two main peaks, known as the D and G bands, located around 1340 and 1570 cm^{-1}, respectively. The D peak is related to disordered symmetry and originates from structural sp^3 defects, edge defects, or dangling carbon bonds.[35] The G band corresponds to in-plane vibrations of a graphitic structure.[36] The D(I)/G(I) ratio represents the mean distance between two defects, known as LD, and offers a quantification of the concentration of defects.[37] Bare graphene has a D(I)/G(I) ratio of 0.79. Interestingly, when graphene is exposed to oxygen plasma, the intensity of the D peak increases while the G peak decreases. The D(I)/G(I) ratio significantly increases, resulting in ratios of 1.58 and 1.41 for 5 and 15 minutes of oxygen plasma exposure, respectively. This suggests the introduction of point defects into the sp^2 lattice, leading to an increase in the density of defects and a reduction in the average distance between them.[38] It is worth noting that the 15-minute plasma exposure shows a slightly lower D(I)/G(I) ratio than the 5-minute exposure, possibly due to the strong amorphization of graphene caused by an excessive density of defects.[38]

A D' peak appears at 1625 cm^{-1} when graphene is exposed to oxygen plasma. This peak is associated with defect-activated bands[39] and becomes more prominent with longer exposure times to oxygen plasma. The 15-minute treatment shows a clearly visible D' band and a significant shoulder at higher Raman shifts. Additionally, the 2D band, also known as the G' band, is observed. This is the second order of the D peak and appears at around 2690 cm^{-1}. Pristine

graphene exhibits a prominent 2D peak, while increasing exposure times to oxygen plasma tend to reduce the intensity of this band, indicating increasing disorder in the graphene lattice due to a higher density of defects.[40]

Figure 3a presents a comparison of the survey spectra obtained from XPS analysis of the untreated graphene and samples exposed to 5 and 15 minutes of plasma. The intensity of the O1s peak increases with longer plasma exposure. Table 1 provides the quantification of the graphene's oxygen content, revealing that the longest plasma treatment results in an oxygen content of 41.3%, compared to 17.9% for the 5-minute exposure. Figure 3b displays the deconvolution of the C1s peak for the graphene with optimal oxygen content, showing the presence of oxygen species such as C-O, C=O, and COOH. Additionally, Figure S3a and Figure S3b show the C1s deconvolution for the other samples, indicating an increase in the density of C-sp^3 and a higher abundance of oxygen species such as carboxylic acid due to the oxygen plasma exposure.

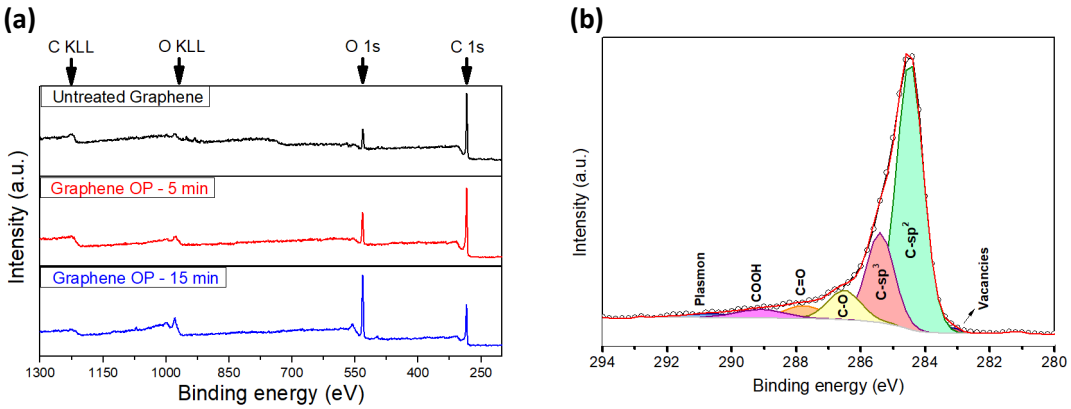

Figure 3. (a) Comparison of XPS survey spectra between bare graphene (black line) and graphene exposed to 5 (red line) and 15 minutes (blue line) of oxygen plasma. (b) XPS analysis of the C1s spectrum for the graphene treated with 5 minutes of plasma.

Table 1. XPS quantification of carbon and oxygen content for the different graphene samples.

	Carbon	**Oxygen**
Untreated Graphene	88.02	11.97
Graphene OP - 5 min	82.11	17.89
Graphene OP - 15 min	58.65	41.35

3.2. Chemiresistive sensing

Oxygen plasma treatments have a significant impact on the graphene lattice, as illustrated in Figure 2b. The baseline resistance of the pristine perovskite-graphene nanocomposite has increased from a few K(Ohms) to several M(Ohms) after 5 minutes of oxygen plasma exposure. It can be expected that 15 minutes of exposure results in an even higher density of defects, vacancies, and disorders in the carbon lattice, which can potentially affect the electrical properties. Consequently, the baseline resistance is further increased, surpassing the measurement capabilities of the employed multimeter and preventing from measuring the sensor response. In the case of bare graphene, its well-known low reactivity makes it challenging to distinguish the sensing response to CO_2 from the noise level, as observed in Figure S4a. Therefore, the subsequent results will mainly focus on the pristine sample (untreated perovskite@graphene) and the sample exposed to 5 minutes of plasma treatment.

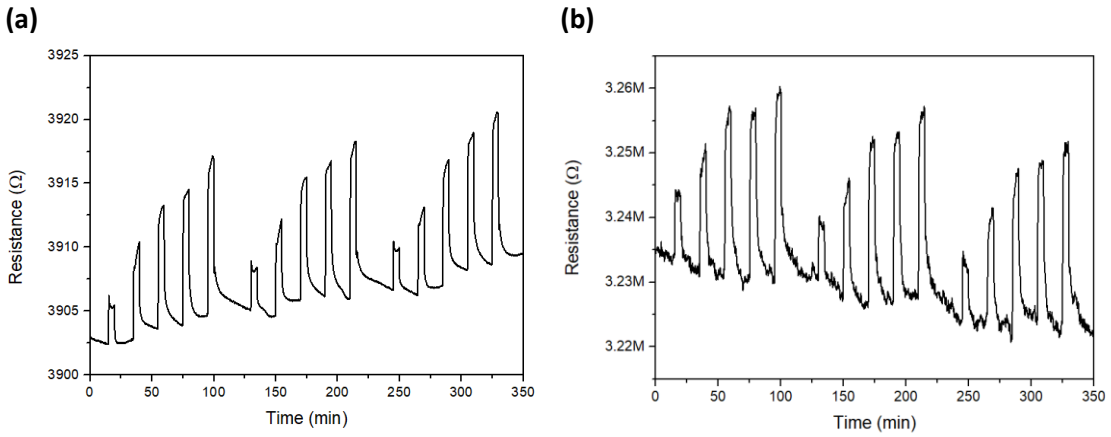

Figure 4. Electrical responses of different nanohybrids while detecting increasing concentrations (20, 40, 60, 80 and 100 ppm) of CO_2 over three consecutive cycles. (a) $CsPbBr_3$ NCs suspended on graphene without plasma treatments. (b) $CsPbBr_3$ NCs suspended on graphene exposed to 5 minutes of oxygen plasma.

The perovskite-graphene hybrids were exposed to various concentrations of CO_2. Figure 4a and Figure 4b illustrate the dynamic changes in resistance observed when exposed to 20, 40, 60, 80, and 100 ppm of CO_2 over three consecutive cycles. Both sensitive films demonstrate effective CO_2 detection within this concentration range. However, Figure 5a reveals that $CsPbBr_3$ nanocrystals suspended on graphene exhibit responses to CO_2 that are up to three times higher when exposed to 5 minutes of oxygen plasma. This enhancement is particularly noticeable at lower concentration levels, ranging from 20 to 60 ppm of CO_2. The slight drift in the baseline observed in Figure 4 does not compromise the repeatability of the sensing responses, as demonstrated in Figure 5b. This graph presents ten consecutive responses to 50 ppm of CO_2 using the nanohybrid sensor treated with 5 minutes of oxygen plasma. The response and recovery times were set at 5 and 15 minutes, respectively, to maintain consistent experimental conditions. As a result, the $CsPbBr_3$ NCs suspended on graphene and exposed to 5 minutes of oxygen plasma exhibit an experimental error of only 3.8%.

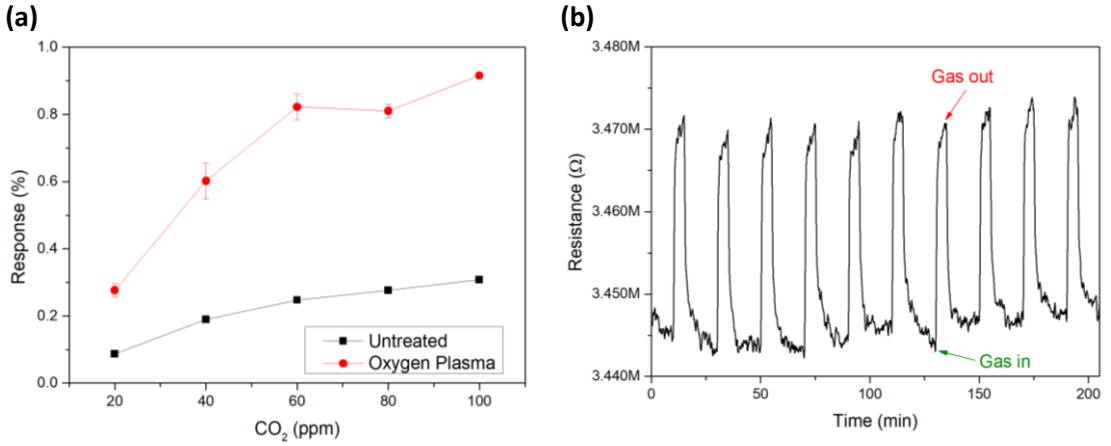

Figure 5. (a) Comparison of the calibration curves obtained for oxygen plasma treated and untreated $CsPbBr_3$ NCs suspended on graphene. (b) Repeatability test applying 10 times 50 ppm of CO_2 and employing the $CsPbBr_3$ NCs suspended on graphene exposed to 5-minute of oxygen plasma.

To properly assess the sensing performance of the perovskite-graphene nanocomposite with oxygen-plasma treatment, it is essential to calculate the limit of detection (LOD) and limit of quantification (LOQ). These values offer insights into the suitability of the developed nanomaterials for real-world applications. The limits can be determined using the following equations:

$$LOD = 3\frac{Sy}{b} \quad (1)$$

$$LOQ = 10\frac{Sy}{b} \quad (2)$$

where *Sy* corresponds to the standard deviation of y-residuals and *b* is the slope of the calibration curve obtained by plotting the sensor response against the CO_2 concentration. The determination of LOD and LOQ is crucial for evaluating the sensing performance of the perovskite-graphene nanocomposite. The LOD represents the lowest detectable concentration of CO_2, indicating its presence in the atmosphere but not allowing for accurate quantification. On the other hand, the LOQ represents the lowest concentration that can be reliably quantified. In the case of the untreated nanocomposite, the LOD is determined to be 20.5 ppm, indicating the minimum CO_2 concentration that can be detected. However, when the nanocomposite is exposed to 5 minutes of oxygen plasma, the LOD is significantly reduced to 6.9 ppm, demonstrating an enhanced sensitivity to CO_2. Similarly, the LOQ for the untreated nanocomposite is determined to be 68.3 ppm. In contrast, the nanocomposite exposed to 5 minutes of oxygen plasma achieves a lower LOQ of 22.9 ppm, indicating an improved ability to accurately quantify CO_2 concentrations. These calculations highlight the superior sensing performance of the perovskite-graphene nanocomposite when treated with 5 minutes of oxygen plasma. The LOD and LOQ values are reduced by approximately three times, indicating the effectiveness of this clean, fast, and reagent-free treatment in enhancing the nanocomposite's sensing capabilities.

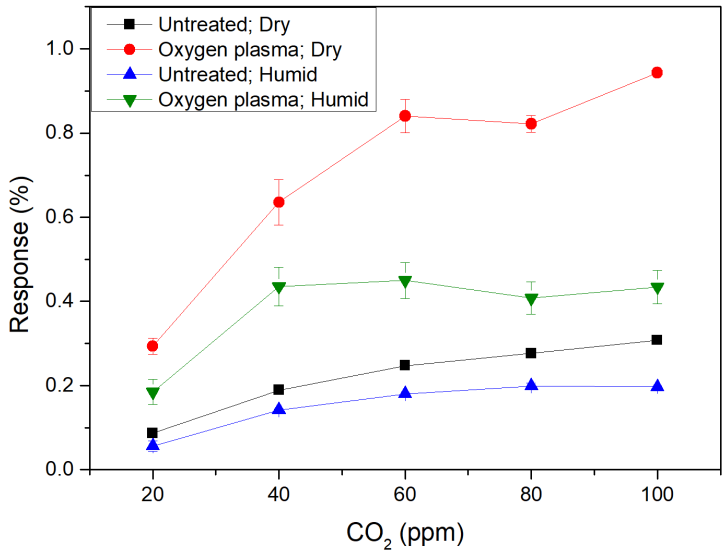

Figure 6. Comparison of the calibration curves obtained for $CsPbBr_3$ NCs suspended on graphene with and without oxygen plasma treatment, and under both dry and humid atmospheric conditions.

The presence of water molecules in the atmosphere is a major interference factor in chemiresistive gas sensors. Therefore, it is important to evaluate the ability to detect CO_2 in a

humid environment. In this study, a constant relative humidity of 80% was maintained during the sensing measurements, including both the recovery and response steps. Figure S4b presents dynamic response examples obtained when detecting CO_2 in the concentration range of 20-100 ppm under humid conditions. It is observed that the resistance baseline has significantly decreased, indicating the influence of water molecules as electron-withdrawing species. While an electron-donor nature of water cannot be completely ruled out, Hall measurements have shown that water tends to act as an electron-withdrawing molecule when interacting with graphene, particularly at room temperature.[41,42]

Figure 6 provides a comparison of the responses in a dry atmosphere and a humid atmosphere. It is important to highlight that both the untreated and oxygen plasma-treated perovskite-graphene nanocomposites exhibit a decrease in sensing performance in the presence of ambient moisture. This behavior can be attributed to several factors. Firstly, it has been reported in previous studies that the presence of water molecules tends to hinder the adsorption of CO_2 on carbonaceous nanomaterials, particularly affecting the interaction between oxygen-containing functional groups and CO_2.[43,44] Secondly, water molecules can passivate the perovskite, leading to significantly lower charge transport and limiting the radiative recombination of electron-hole pairs.[45,46]

It is worth noting that the untreated hybrid shows a moderate decrease in sensing performance under humid conditions. However, the nanocomposite treated with 5 minutes of oxygen plasma exhibits a significant decrease compared to its non-plasma-exposed counterpart. This is likely due to the removal of unbound surface ligands by the oxygen plasma, exposing the $CsPbBr_3$ perovskite to water molecules and amplifying the effect of ambient moisture.[32]

3.3. Optical studies

In pursuit of a deeper understanding of the sensing mechanisms, photoluminescent (PL) studies were undertaken. PL studies serve as a sensitive tool for delving into how materials interact within their surroundings and revealing the presence of defects. In this perspective, both steady-state and lifetime photoluminescence measurements were executed directly upon the deposited microelectrodes.

Figure 7 illustrates the PL spectrum of $CsPbBr_3$ NCs, which are supported on graphene without plasma treatment and after exposure to oxygen plasma for 5 and 15 minutes. It becomes evident that both samples exposed to oxygen plasma yield a noticeable decrease in luminescence intensity. This decrease in peak intensity is commonly associated with the removal of organic ligands from the surface. Nevertheless, it is crucial to acknowledge that prolonged exposure, lasting 15 minutes, can result in the deterioration of $CsPbBr_3$ NCs.[47] The sample treated for 5 minutes exhibits a widening of the maximum emission, as indicated by a Full Width at Half Maximum (FWHM) of 33.98, in contrast to the untreated sample's FWHM of 21.25. This broadening of the emission signifies the emergence of additional defects within the $CsPBBr_3$ NCs.[48,49]

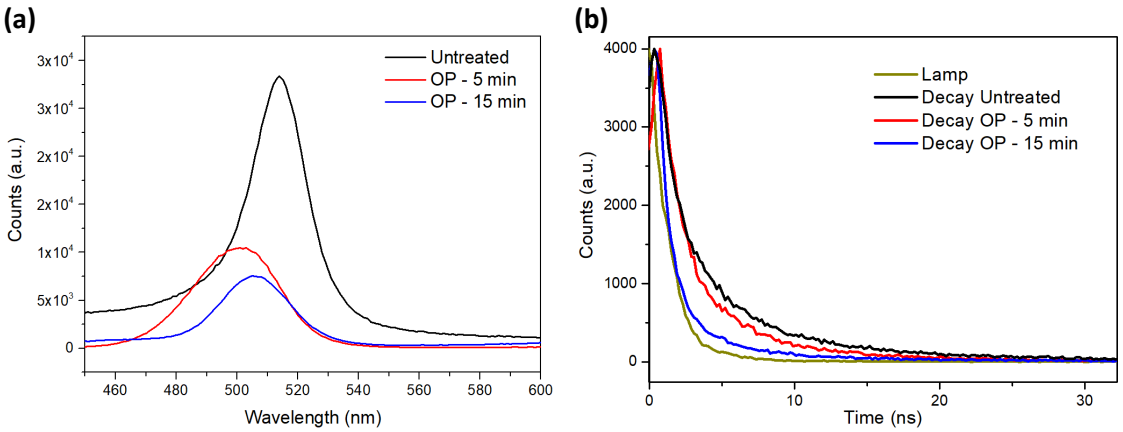

Figure 7. (a) Photoluminescence of $CsPbBr_3$ NCs supported on graphene, both before and after exposure to oxygen plasma for 5 and 15 minutes. (b) Lifetime measurements registered at λ_{ex} = 405 nm and monitored at 550 nm under room conditions.

Concerning the PL decay lifetimes, the best fitting corresponds to a biexponential decay model, where the short lifetime (approximately 1 ns) is attributed to non-radiative recombination of electron-hole pairs.[50] Notably, the percentage contribution of this component (referred to as value A1 in Table 2) becomes increasingly significant as the duration of oxygen plasma treatment extends. This accelerated decay, coupled with the reduction of the PL intensity (Figure 7a), suggests that surface defects in the NCs are formed following the oxygen plasma treatment.

Table 2. Best-fit parameters for the PL decay profiles of $CsPbBr_3$ NCs. These measurements were taken at emission peak energies, as depicted in Figure 7b, using a bi-exponential decay model for the conditions before oxygen plasma treatment, after 5 minutes, and after 15 minutes. A_1 and A_2 represent the percentage contributions of lifetimes from τ_1 and τ_2, respectively.

Oxygen-plasma treatment time (min)	τ_1	A_1	τ_2	A_2
0	1.56	68.33	6.21	31.67
5	1.32	76.48	5.15	23.52
15	1.03	91.56	5.83	8.44

3.4. Sensing mechanism

The chemiresistive response of this hybrid material is mainly associated with the generation of electron-hole pairs in the perovskite nanocrystals (NCs) when exposed to gases.[51] This response is influenced by both the quantity and type of majority carriers within the film, which directly impact the measured resistance. Regarding the enhanced performance of the hybrid material following a 5-minute oxygen plasma treatment, two factors are believed to be involved.

First, the plasma treatment leads to a reduction of excess organic ligands.[32] These ligands, which can be unbound long-chain molecules present during synthesis, may potentially isolate the surface of the nanocrystals (NCs). Thereby, partial removal of these ligands facilitates a cleaner NC structure, increasing the available active surface area for gas interaction and promoting carrier transport at the interface with the graphene layers. Secondly, changes observed in the

photoluminescence (PL) signal after the 5-minute oxygen plasma treatment indicate the formation of additional defects. These defects serve as active centres and enhance the accessibility of active sites, enabling stronger interactions with CO_2.

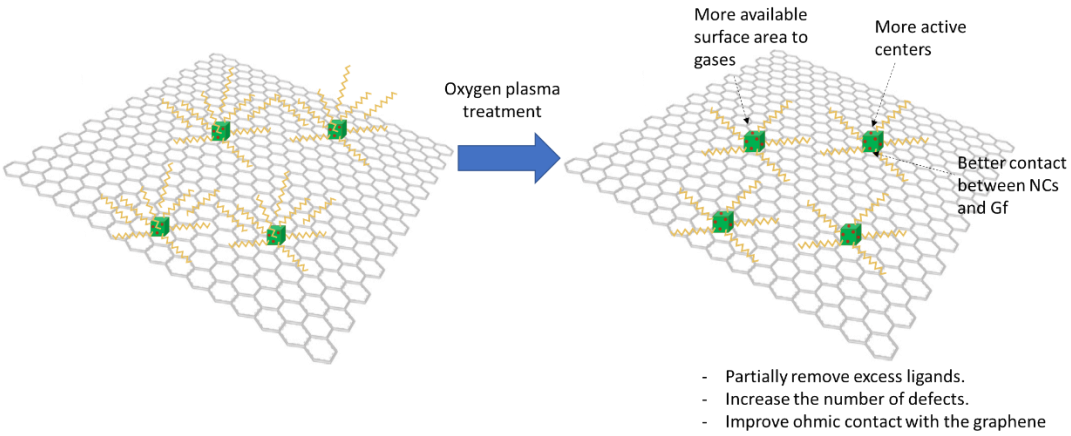

Figure 8. Representation of the oxygen plasma treatment applied to the surface of the studied nanohybrid material.

Nonetheless, the possibility of interactions between graphene and CO_2 cannot be ruled out, particularly when the carbonaceous nanomaterial is exposed to oxygen plasma. Essentially, pristine graphene demonstrates notable inertness towards CO_2 molecules. However, exposure to plasma treatment generates a substantial number of defects, particularly carbon vacancies, creating potential sites for atmospheric oxygen adsorption. Consequently, CO_2 can interact with the oxygen species adsorbed to the graphene surface, leading to the formation of carbonates (as depicted in equations [1] and [2]). Consequently, these adsorbed carbonates can introduce electrons into the sensitive film, resulting in an increase of the resistance.[52,53]

$$CO_{2\,(gas)} + O^-_{(ads)} \leftrightarrow CO_3^-{}_{(ads)} \quad [1]$$

$$CO_{2\,(gas)} + 2O^-_{(ads)} \leftrightarrow CO_3^{2-}{}_{(ads)} \quad [2]$$

4. Conclusions

The detrimental impact of CO_2 on the environment and human health is widely acknowledged, necessitating advanced sensors capable of detecting this pollutant across diverse environments. However, addressing challenges such as cost-effectiveness, user-friendliness, stability, and low power consumption remains crucial. This study introduces a novel chemiresistive sensor comprising perovskite nanocrystals supported on graphene, and treated with plasma, a rapid and reagent-free method for enhancing sensor performance.

Oxygen plasma is a powerful tool for engineering surface defects and introducing oxygen-related groups. While these defects and oxygen vacancies could be detrimental in certain applications like photovoltaics, they proved advantageous in chemiresistive sensors to some extent. Thus, several durations of oxygen plasma exposure were explored, revealing a threefold enhancement in sensing performance after a 5-minute treatment compared to untreated films.

Consequently, oxygen plasma-treated perovskite nanocrystals on graphene demonstrated remarkable potential for room temperature CO_2 sensing, significantly improving sensitivity and reducing critical parameters like LOD and LOQ. Although atmospheric humidity impacted sensor

performance, the treated composites still outperformed their untreated counterparts. These findings underscore the efficacy of these developed nanocomposites for real-world applications.

5. References

(1) Frank, D. A.; Becklin, K. M.; Penner, J. F.; Lindsay, K. A.; Geremia, C. J. Feast or Famine: How Is Global Change Affecting Forage Supply for Yellowstone's Ungulate Herds? *Ecol. Appl.* **2023**, *33* (1), e2735.

(2) Assen, N. Von Der; Müller, L. J.; Steingrube, A.; Voll, P.; Bardow, A. Selecting CO2 Sources for CO2 Utilization by Environmental-Merit-Order Curves. *Environ. Sci. Technol.* **2016**, *50* (3), 1093–1101.

(3) Hunter, S. E.; Lixiong, L.; Doug, D.; Armendinger, T. Improving Water Spray Efficacy for Fire Suppression via CO2 Addition at High Pressures and Low Temperatures: Evidence for CO2 Clathrate Hydrate Formation. *Ind. Eng. Chem. Res.* **2006**, *45* (21), 7275–7286.

(4) Sharp, J. R.; Pierson, W. P.; Brady, C. E. Comparison of CO2- and N2O-Induced Discomfort During Peritoneoscopy Under Local Anesthesia. *Gastroenterology* **1982**, *82* (3), 453–456.

(5) Saint-Eve, A.; Déléris, I.; Aubin, E.; Semon, E.; Feron, G.; Rabillier, J. M.; Ibarra, D.; Guichard, E.; Souchon, I. Influence of Composition (CO2 and Sugar) on Aroma Release and Perception of Mint-Flavored Carbonated Beverages. *J. Agric. Food Chem.* **2009**, *57* (13), 5891–5898.

(6) Reich, P. B.; Hobbie, S. E.; Lee, T. D. Plant Growth Enhancement by Elevated CO2 Eliminated by Joint Water and Nitrogen Limitation. *Nat. Geosci.* **2014**, *7* (12), 920–924.

(7) Jacobson, T. A.; Kler, J. S.; Hernke, M. T.; Braun, R. K.; Meyer, K. C.; Funk, W. E. Direct Human Health Risks of Increased Atmospheric Carbon Dioxide. *Nat. Sustain.* **2019**, *2* (8), 691–701.

(8) Lyu, X.; Luo, Z.; Shao, L.; Awbi, H.; Lo Piano, S. Safe CO2 Threshold Limits for Indoor Long-Range Airborne Transmission Control of COVID-19. *Build. Environ.* **2023**, *234*, 109967.

(9) Peng, Z.; Jimenez, J. L. Exhaled CO2 as a COVID-19 Infection Risk Proxy for Different Indoor Environments and Activities. *Environ. Sci. Technol. Lett.* **2021**, *8* (5), 392–397.

(10) Li, B.; Cai, W. A Novel CO2-Based Demand-Controlled Ventilation Strategy to Limit the Spread of COVID-19 in the Indoor Environment. *Build. Environ.* **2022**, *219*, 109232.

(11) Chocarro-Ruiz, B.; Pérez-Carvajal, J.; Avci, C.; Calvo-Lozano, O.; Alonso, M. I.; Maspoch, D.; Lechuga, L. M. A CO2 Optical Sensor Based on Self-Assembled Metal–Organic Framework Nanoparticles. *J. Mater. Chem. A* **2018**, *6* (27), 13171–13177.

(12) Wang, C.; Ding, Y.; Li, M.; Li, H.; Xu, S.; Li, C.; Qian, L.; Yang, B. Surface Acoustic Wave Sensor Based on Au/TiO2/PEDOT with Dual Response to Carbon Dioxide and Humidity. *Anal. Chim. Acta* **2022**, *1190*, 339264.

(13) Muraoka, S.; Kiyohara, Y.; Oue, H.; Higashimoto, S. A CO2 Sensor Using a Quartz Crystal Microbalance Coated with a Sensitive Membrane. *Electron. Commun. Japan* **2014**, *97* (2), 60–66.

(14) Koo, W. T.; Cho, H. J.; Kim, D. H.; Kim, Y. H.; Shin, H.; Penner, R. M.; Kim, I. D.

Chemiresistive Hydrogen Sensors: Fundamentals, Recent Advances, and Challenges. *ACS Nano* **2020**, *14* (11), 14284–14322.

(15) Karthik, T. V. K.; Martinez, L.; Agarwal, V. Porous Silicon ZnO/SnO2 Structures for CO2 Detection. *J. Alloys Compd.* **2018**, *731*, 853–863.

(16) Jeong, Y. J.; Balamurugan, C.; Lee, D. W. Enhanced CO2 Gas-Sensing Performance of ZnO Nanopowder by La Loaded during Simple Hydrothermal Method. *Sensors Actuators B Chem.* **2016**, *229*, 288–296.

(17) Kanaparthi, S.; Singh, S. G. Chemiresistive Sensor Based on Zinc Oxide Nanoflakes for CO2 Detection. *ACS Appl. Nano Mater.* **2019**, *2* (2), 700–706.

(18) Korotcenkov, G. Gas Response Control through Structural and Chemical Modification of Metal Oxide Films: State of the Art and Approaches. *Sensors Actuators B Chem.* **2005**, *107* (1), 209–232.

(19) Ghosh, R.; Gardner, J. W.; Guha, P. K. Air Pollution Monitoring Using Near Room Temperature Resistive Gas Sensors: A Review. *IEEE Trans. Electron Devices* **2019**, *66* (8), 3254–3264.

(20) Majhi, S. M.; Mirzaei, A.; Kim, H. W.; Kim, S. S.; Kim, T. W. Recent Advances in Energy-Saving Chemiresistive Gas Sensors: A Review. *Nano Energy* **2021**, *79*, 105369.

(21) Fu, W.; Jiang, L.; van Geest, E. P.; Lima, L. M. C.; Schneider, G. F. Sensing at the Surface of Graphene Field-Effect Transistors. *Adv. Mater.* **2017**, *29* (6), 1603610.

(22) Wang, L. Q.; Ma, H. H.; Shen, Z. W. Explosion Characteristics of Hydrogen-Air Mixtures Diluted with Inert Gases at Sub-Atmospheric Pressures. *Int. J. Hydrogen Energy* **2019**, *44* (40), 22527–22536.

(23) Salih, E.; Ayesh, A. I. CO, CO2, and SO2 Detection Based on Functionalized Graphene Nanoribbons: First Principles Study. *Phys. E Low-dimensional Syst. Nanostructures* **2020**, *123*, 114220.

(24) Zhang, C.; Xu, K.; Liu, K.; Xu, J.; Zheng, Z. Metal Oxide Resistive Sensors for Carbon Dioxide Detection. *Coord. Chem. Rev.* **2022**, *472*, 214758.

(25) Choi, J. H.; Lee, J.; Byeon, M.; Hong, T. E.; Park, H.; Lee, C. Y. Graphene-Based Gas Sensors with High Sensitivity and Minimal Sensor-to-Sensor Variation. *ACS Appl. Nano Mater.* **2020**, *3* (3), 2257–2265.

(26) Casanova-Chafer, J.; Garcia-Aboal, R.; Atienzar, P.; Llobet, E. Unraveling the Gas-Sensing Mechanisms of Lead-Free Perovskites Supported on Graphene. *ACS Sensors* **2022**, *7* (12), 3753–3763.

(27) Casanova-Cháfer, J.; García-Aboal, R.; Atienzar, P.; Llobet, E. Gas Sensing Properties of Perovskite Decorated Graphene at Room Temperature. *Sensors* **2019**, *19* (20), 4563.

(28) Bianco, G. V.; Sacchetti, A.; Ingrosso, C.; Giangregorio, M. M.; Losurdo, M.; Capezzuto, P.; Bruno, G. Engineering Graphene Properties by Modulated Plasma Treatments. *Carbon N. Y.* **2018**, *129*, 869–877.

(29) Wu, H.; Bu, X.; Deng, M.; Chen, G.; Zhang, G.; Li, X.; Wang, X.; Liu, W. A Gas Sensing Channel Composited with Pristine and Oxygen Plasma-Treated Graphene. *Sensors* **2019**, *19* (3), 625.

(30) Zhang, S.; Pang, J.; Li, Y.; Ibarlucea, B.; Liu, Y.; Wang, T.; Liu, X.; Peng, S.; Gemming, T.;

Cheng, Q.; Liu, H.; Yang, J.; Cuniberti, G.; Zhou, W.; Rümmeli, M. H. An Effective Formaldehyde Gas Sensor Based on Oxygen-Rich Three-Dimensional Graphene. *Nanotechnology* **2022**, *33* (18), 185702.

(31) Lien, S. Y.; Wang, C. W.; Chen, W. R.; Liu, C. H.; Kang, C. C.; Huang, C. J. The Influence of Oxygen Plasma on Methylammonium Lead Iodide (MAPbI3) Film Doped with Lead Cesium Triiodide (CsPbI3). *Molecules* **2021**, *26* (17), 5133.

(32) Palazon, F.; Chen, F.; Akkerman, Q. A.; Imran, M.; Krahne, R.; Manna, L. Effects of Oxygen Plasma on the Chemical, Light-Emitting, and Electrical-Transport Properties of Inorganic and Hybrid Lead Bromide Perovskite Nanocrystal Films. *ACS Appl. Nano Mater.* **2018**, *1* (10), 5396–5400.

(33) Protesescu, L.; Yakunin, S.; Bodnarchuk, M. I.; Krieg, F.; Caputo, R.; Hendon, C. H.; Yang, R. X.; Walsh, A.; Kovalenko, M. V. Nanocrystals of Cesium Lead Halide Perovskites (CsPbX3, X = Cl, Br, and I): Novel Optoelectronic Materials Showing Bright Emission with Wide Color Gamut. *Nano Lett.* **2015**, *15* (6), 3692–3696.

(34) Casanova-Chafer, J.; Umek, P.; Acosta, S.; Bittencourt, C.; Llobet, E. Graphene Loading with Polypyrrole Nanoparticles for Trace-Level Detection of Ammonia at Room Temperature. *ACS Appl. Mater. Interfaces* **2021**, *13* (34), 40909–40921.

(35) Sebastian, F. L.; Zorn, N. F.; Settele, S.; Lindenthal, S.; Berger, F. J.; Bendel, C.; Li, H.; Flavel, B. S.; Zaumseil, J. Absolute Quantification of Sp3Defects in Semiconducting Single-Wall Carbon Nanotubes by Raman Spectroscopy. *J. Phys. Chem. Lett.* **2022**, *13* (16), 3542–3548.

(36) Dubale, A. A.; Su, W. N.; Tamirat, A. G.; Pan, C. J.; Aragaw, B. A.; Chen, H. M.; Chen, C. H.; Hwang, B. J. The Synergetic Effect of Graphene on Cu2O Nanowire Arrays as a Highly Efficient Hydrogen Evolution Photocathode in Water Splitting. *J. Mater. Chem. A* **2014**, *2* (43), 18383–18397.

(37) Cançado, L. G.; Jorio, A.; Ferreira, E. H. M.; Stavale, F.; Achete, C. A.; Capaz, R. B.; Moutinho, M. V. O.; Lombardo, A.; Kulmala, T. S.; Ferrari, A. C. Quantifying Defects in Graphene via Raman Spectroscopy at Different Excitation Energies. *Nano Lett.* **2011**, *11* (8), 3190–3196.

(38) Felten, A.; Eckmann, A.; Pireaux, J. J.; Krupke, R.; Casiraghi, C. Controlled Modification of Mono- and Bilayer Graphene in O2, H2 and CF4 Plasmas. *Nanotechnology* **2013**, *24* (35), 355705.

(39) Xia, W.; Tang, J.; Li, J.; Zhang, S.; Wu, K. C.-W.; He, J.; Yamauchi, Y. Defect-Rich Graphene Nanomesh Produced by Thermal Exfoliation of Metal–Organic Frameworks for the Oxygen Reduction Reaction. *Angew. Chemie* **2019**, *131* (38), 13488–13493.

(40) Ferrari, A. C. Raman Spectroscopy of Graphene and Graphite: Disorder, Electron–Phonon Coupling, Doping and Nonadiabatic Effects. *Solid State Commun.* **2007**, *143* (1–2), 47–57.

(41) Schedin, F.; Geim, A. K.; Morozov, S. V.; Hill, E. W.; Blake, P.; Katsnelson, M. I.; Novoselov, K. S. Detection of Individual Gas Molecules Adsorbed on Graphene. *Nat. Mater.* **2007**, *6* (9), 652–655.

(42) Knight, S.; Hofmann, T.; Bouhafs, C.; Armakavicius, N.; Kühne, P.; Stanishev, V.; Ivanov, I. G.; Yakimova, R.; Wimer, S.; Schubert, M.; Darakchieva, V. In-Situ Terahertz Optical Hall Effect Measurements of Ambient Effects on Free Charge Carrier Properties of

Epitaxial Graphene. *Sci. Rep.* **2017**, *7* (1), 1–8.

(43) Liu, Y.; Wilcox, J. Effects of Surface Heterogeneity on the Adsorption of CO2 in Microporous Carbons. *Environ. Sci. Technol.* **2012**, *46* (3), 1940–1947.

(44) Lin, Y.; Fan, Z. Compositing Strategies to Enhance the Performance of Chemiresistive CO2 Gas Sensors. *Mater. Sci. Semicond. Process.* **2020**, *107*, 104820.

(45) Zhou, H.; Park, J.; Lee, Y.; Park, J. M.; Kim, J. H.; Kim, J. S.; Lee, H. D.; Jo, S. H.; Cai, X.; Li, L.; Sheng, X.; Yun, H. J.; Park, J. W.; Sun, J. Y.; Lee, T. W. Water Passivation of Perovskite Nanocrystals Enables Air-Stable Intrinsically Stretchable Color-Conversion Layers for Stretchable Displays. *Adv. Mater.* **2020**, *32* (37), 2001989.

(46) Fang, H. H.; Adjokatse, S.; Wei, H.; Yang, J.; Blake, G. R.; Huang, J.; Even, J.; Loi, M. A. Ultrahigh Sensitivity of Methylammonium Lead Tribromide Perovskite Single Crystals to Environmental Gases. *Sci. Adv.* **2016**, *2* (7).

(47) Rathod, R.; Das, R.; Das, M. R.; Santra, P. K. Plasma-Treated CsPbBr3Nanocrystal Films for Anticounterfeiting Applications. *ACS Appl. Nano Mater.* **2022**, *5* (7), 9852–9860.

(48) Yin, J.; Naphade, R.; Gutiérrez Arzaluz, L.; Brédas, J. L.; Bakr, O. M.; Mohammed, O. F. Modulation of Broadband Emissions in Two-Dimensional <100>-Oriented Ruddlesden-Popper Hybrid Perovskites. *ACS Energy Lett.* **2020**, *5* (7), 2149–2155.

(49) Zhou, G.; Su, B.; Huang, J.; Zhang, Q.; Xia, Z. Broad-Band Emission in Metal Halide Perovskites: Mechanism, Materials, and Applications. *Mater. Sci. Eng. R Reports* **2020**, *141*, 100548.

(50) Kumawat, N. K.; Swarnkar, A.; Nag, A.; Kabra, D. Ligand Engineering to Improve the Luminance Efficiency of CsPbBr3 Nanocrystal Based Light-Emitting Diodes. *J. Phys. Chem. C* **2018**, *122* (25), 13767–13773.

(51) Casanova-Chafer, J.; Garcia-Aboal, R.; Atienzar, P.; Llobet, E. The Role of Anions and Cations in the Gas Sensing Mechanisms of Graphene Decorated with Lead Halide Perovskite Nanocrystals. *Chem. Commun.* **2020**, *56* (63), 8956–8959.

(52) Nemade, K. R.; Waghuley, S. A. Chemiresistive Gas Sensing by Few-Layered Graphene. *J. Electron. Mater.* **2013**, *42* (10), 2857–2866.

(53) Nemade, K. R.; Waghuley, S. A. Role of Defects Concentration on Optical and Carbon Dioxide Gas Sensing Properties of Sb2O3/Graphene Composites. *Opt. Mater. (Amst).* **2014**, *36* (3), 712–716.